İSTANBUL TECHNICAL UNIVERSITY ★ INFORMATICS INSTITUTE

SVD INVERSION TECHNIQUE FOR THE RECONSTRUCTION OF BURIED OBJECTS

M.Sc. Thesis by

Evrim TETİK, B.Sc.

Department : Advanced Technologies in Engineering

Programme: Satellite Remote Sensing and Communication

JUNE 2007

İSTANBUL TECHNICAL UNIVERSITY ★ INFORMATICS INSTITUTE

SVD INVERSION TECHNIQUE FOR THE RECONSTRUCTION OF BURIED OBJECTS

M.Sc. Thesis by

Evrim TETİK, B.Sc.

(705051001)

Date of submission : 7 May 2007

Date of defence examination: 12 June 2007

Supervisor (Chairman): Prof. Dr. İbrahim AKDUMAN

Co-Supervisor: Dr. Lorenzo CROCCO

Members of the Examining Committee Prof.Dr. İrşadi AKSUN (KÜ.)

Assoc. Prof.Dr. Ali YAPAR (İ.T.Ü.)

Assist.Prof.Dr. Lale Tükenmez ERGENE (İ.T.Ü.)

JUNE 2007

İSTANBUL TEKNİK ÜNİVERSİTESİ ★ BİLİŞİM ENSTİTÜSÜ

GÖMÜLÜ CİSİMLERİN TEKİL DEĞER AYRIŞTIRMA TEKNİĞİ KULLANILARAK BULUNMASI

YÜKSEK LİSANS TEZİ

Müh. Evrim TETİK
(705051001)

Tezin Enstitüye Verildiği Tarih : 7 Mayıs 2007
Tezin Savunulduğu Tarih : 12 Haziran 2007

Tez Danışmanı :	**Prof.Dr. İbrahim AKDUMAN**
Tez Eş Danışmanı:	**Dr. Lorenzo CROCCO**
Diğer Jüri Üyeleri	**Prof.Dr. İrşadi AKSUN (K.Ü.)**
	Doç.Dr. Ali YAPAR (İ.T.Ü.)
	Y.Doç.Dr. Lale Tükenmez ERGENE (İ.T.Ü.)

HAZİRAN 2007

TABLE OF CONTENT

LIST OF ABBREVIATIONS

GPR	: Ground Penetrating Radar
BA	: Born Approximation
SVD	: Singular Value Decomposition
SNR	: Signal to Noise Ratio
SF	: Single Frequency
MF	: Multi Frequency
Tx	: Transmitter
Rx	: Receiver

LIST OF FIGURES

LIST OF SYMBOLS

ε_0	: Dielectric permittivity of the free space
μ_0	: Magnetic permeability of the free space
$\varepsilon_1, \varepsilon_2, \varepsilon_3,$	: Relative dielectric permittivities of the first, second and the third media, respectively.
ε_D	: Relative dielectric permittivity of the contrast
ε_i	: Generic relative dielectric permittivity
ε_i^{eq}	: Generic complex equivalent relative dielectric permittivity
$\sigma_1, \sigma_2, \sigma_3$	: Conductivities of first, second and the third media, respectively
σ_D	: Conductivity of the contrast
σ_i	: Generic conductivity
$k_1, k_2, k_3,$	: Wavenumbers of the first, second and the third media, respectively.
d	: Width of the slab
f	: Frequency
ω	: Angular frequency
ω_m	: Maximum working frequency
Γ	: Antenna array
$\bar{\mathbf{E}}$	: Vectoral total field in whole space
$\mathbf{E}^0$	: Total field in whole space in the absence of the buried objects
$\mathbf{E}$	: Total field
$\mathbf{E}^s$	: Scattered field due to the buried objects
χ	: Contrast function
G	: Green's function of the three part space
$\hat{G}$	: Fourier transform of G
$\mathbf{r}$	: generic observation point
$\mathbf{r'}$	: generic source point
$\mathbf{r}_r$	: Observation point located in the first medium
$\mathbf{r}_t$	: Source point located in the reconstruction domain
ν	: Spatial frequency
δ	: Dirac delta distribution
σ_n	: singular values

ÖZET

Tomografik yaklaşım, elde edilen GPR verisine anlam kazandırarak, test edilen bölgeye ilişkin nitelikli bilgi elde etme konusunda önemli bir yere sahiptir. Bu tez çalışmasında, bir tabaka içine gömülü dielektrik cisimlerin görüntülenmesi için, lineerleştirilmiş bir tomografik yaklaşım kullanılmıştır. Problem, verinin sonlu uzunlukta lineer bir çizgi üzerinde toplandığı iki boyutlu bir geometri ve skaler bir duruma dayanılarak ele alınmıştır. Özellikle kullanılabilir bağımsız veri miktarını arttırmak için birden çok frekanslı, çok aydınlatma ve ölçüm konumlu bir ölçüm konfigürasyonu göz önüne alınmıştır. Bu demektir ki gömülü cisimlerden saçılan elektrik alan, her bir çalışma frekansı ve verici anten konumu için aynı çizgi üzerinde farklı yerlerdeki alıcı antenler tarafından ölçülmektedir.

Ele alınan yöntem Born yaklaşıklığı ve Tekil Değer Ayrıştırması (SVD) kullanılarak yapılan regülarizasyona dayanmaktadır. Tekil Değer Ayrıştırmasına dayanan sayısal analizler yardımıyla çalışma frekansı, verici ve alıcı anten sayısı gibi ölçüm konfigürasyonu parametrelerinin de nasıl optimize edilebileceği incelenmiştir.

Ele alınan yöntemin veri üzerinde gürültü olduğu durumlarda dahi ne kadar etkili ve sağlıklı sonuçlar verdiği, sayısal örneklerden yararlanılarak test edilmiştir.

SUMMARY

The tomographic approach appears to be a promising way to elaborate Ground Penetrating Radar (GPR) data in order to achieve quantitative information on the tested regions. In this thesis we apply a linearized tomographic approach to the reconstruction of dielectric objects embedded in a layered medium. The problem is tackled with reference to a two-dimensional geometry and scalar case wherein the data are collected over a linear domain with finite extent. In particular, in order to increase the amount of independent available data, a multi-frequency/multi-view/multi-static measurement configuration is considered. With reference to Stepped-Frequency radar systems, this means that for each working frequency and for each position of the transmitting antenna (moved along a linear domain), the electric field scattered by the buried targets is measured in several locations along the same linear domain. The considered inversion approach is based on the Born approximation and a regularized solution is introduced by means of the Singular Value Decomposition. The problem of determining the optimal measurement configuration (in terms of number of frequencies and number of transmitting and receiving antennas) is also faced via a numerical analysis relying on the Singular Value Decomposition. Numerical examples are provided to assess effectiveness and robustness of the proposed approach against noise on data.

1. INTRODUCTION

The Ground Penetrating Radar (GPR) is largely employed in civil engineering, shallow subsurface prospecting applications and archaeology [1], since it allows to perform a non invasive diagnostics of the probed domain in a fast and simple way.

GPR works by emitting a modulated electromagnetic pulse into the ground and by recording the strength of the echo, produced by the interaction between the impinging waves and the buried objects, received at the air-soil interface in a monostatic or bistatic configuration. In the former case the locations of the transmitting and the receiving antennas are coincident, whereas they are different in the latter case. By moving the antenna along a selected profile above the ground surface a two-dimensional plot (radargram) is obtained in which the delay time of the recorded echoes (which can be related to the depth of the underground reflectors) is drawn versus the antenna position [1].

This fast and simple operating mode is however able to survey only the presence and the location of the buried object, but not its characteristics, unless additional a priori information are provided. Moreover, since it is usually based on the assumption that the velocity of the investigating wave is constant, it may often give misleading results. Finally, the interpretation of the radargrams is itself a difficult task which encompasses the ability and the expertise of the user and requires the availability of a priori information about the domain under investigation.

A tomographic approach represents a possible way to overcome these limitations as it makes it possible to achieve *quantitative* reconstruction of the domain under investigation, in terms of location, shape and possibly chemical / physical properties of the buried targets [2,3]. In this case, the problem at hand amounts to determining the dielectric and conductive properties of the probed domain starting from the knowledge of the electromagnetic field scattered under the incidence of known impinging fields.

To this aim one has to perform the inversion of a pair of coupled integral equations which govern the electromagnetic scattering. Such an inversion is not a simple task since it consists in solving a non-linear ill-posed inverse problem [4]. Indeed, due to the properties of the kernel of the integral equation relating the unknowns to the scattered field data [4,5,6], in presence of uncertainties on the data only a finite amount of independent information about the unknowns can be achieved. From a mathematical point of view, this means that a proper regularization strategy has to be adopted in order to restore the well-posedness of the problem [7].

In addition, the nonlinear relationship between the data and the unknowns makes it very difficult to solve the problem, that is usually cast as the minimization of a non quadratic cost functional. This means that this cost functional may exhibit a large number of local optima which corresponds to situations which, being deeply different from the actual solution, are hence denoted as "false solutions". Therefore, to solve the inverse scattering problem one has to be able to achieve the global optimum of the above-mentioned cost functional.

A convenient way to pursue this aim would be that of using "global" optimization methods, which, by their very definition, are such to provide the desired global optimum. Unfortunately, due to the large number of unknowns one usually has to deal with in this kind of problems, this class of approaches, which are based on stochastic tools, are not viable, since their computational cost, which grows exponentially fast with the number of unknown parameters, is not affordable. As a consequence, deterministic minimization techniques have to be adopted [8,9]. However, convergence of deterministic approaches to the global optimum is not ensured as, depending on the adopted starting point the minimization can get stuck into a local minimum of the cost functional. Therefore, these approaches are prone to the occurrence of false solutions, which may impair their usefulness. [8,10]. As a possible strategy to mitigate the local minima problem, one should make the number of the searched parameters as low as possible, or that is equivalent to keep as high as possible the ratio between the amount of independent data and the number of the unknowns to be determined [11]. However, also these strategies have several drawbacks. As a matter of fact, they require for their implementation, the availability of some a priori information about the features of the

unknowns, which is not always the case. Moreover, even when this knowledge is available their effectiveness is limited by constraints on the extent of the probed domain, as they can only tackle with investigated regions whose size is in the order of the wavelength.

The above discussion shows that it is very difficult to tackle the solution of the inverse scattering problem under general conditions. For this reason, another class of solution algorithms has been long investigated in the open literature [2,12,13,14], wherein the adoption of linear approximations of the electromagnetic scattering is considered in order to face a simpler problem. As a matter of fact, linearized inversion algorithms require lower computational cost with respect to the nonlinear ones and no local minima problem arises for the corresponding functionals. The above factors make the linear inversion algorithms suitable in several applications concerning the diagnostics of large probed domain and allow to perform a real-time processing. Conversely, the adoption of approximated models of the electromagnetic scattering, introduces several limitations on the set of unknown functions which can be dealt with [12]. Moreover, unless the considered approximation is almost exactly matched, no information on the electromagnetic characteristics of targets can be obtained. Nevertheless, due to their simplicity and generality linearized inversion approaches appears to be convenient to tackle the problem of subsurface imaging from GPR data.

In microwave tomography, the linearization is usually achieved by means of the Born approximation (BA), which consists in approximating the total electric field inside the investigation domain with the incident one, i.e. the scattering object is a small perturbation with respect to the host medium. This assumption entails some constraints about the extent of the buried objects (which must be small with respect to the investigating wavelength) and on the difference between the dielectric properties of the objects and that of the background medium (which must be as low as possible) [15].

In addition, also within the validity of the Born model, further constraints arise about the unknowns which can be dealt with. These limitations concern their allowable spatial variations and are due to the filtering effect of the relevant linear operator relating the unknowns to the scattered field data [16,13,17]. To this end, the Singular Value

Decomposition (SVD) of the relevant linear compact operator [7] provides a powerful tool to examine the amount of independent information carried by data, to discuss about the class of the retrievable unknowns, to determine the achievable spatial resolution limits in the retrieved tomographic images [16,13,17] and to give a stable solution of the problem.

In this thesis we consider the application of the BA linear approach to the reconstruction of the spatial map of the dielectric and/or conductive properties of an investigation domain in the case of a layered medium. In particular, we consider a three-layered medium and inquire about the dielectric and conductive characteristics of an investigation domain completely embedded in the second layer. Such a scheme is representative of several realistic cases such as for instance masonry diagnostics and prospecting of the shallower layers of soil [18]. The two-dimensional and scalar case is tackled with a filamentary excitation and the data are collected according to a multifrequency / multiview / multistatic strategy. As such, for each working frequency and for each position of the source, the data are measured in several locations along a linear domain of finite extent and very close to the first interface. The only a priori information about the problem regards the location and the extent of the investigation domain within which the objects are supposed to reside.

The organization of the thesis is as follows: In section 2, a general formulation of the inverse scattering problem is formulated. After the details of the linearized tomographic approach are given in the section 3, numerical results are given in section 4, and a conclusion is presented in section 5.

2. FORMULATION OF THE PROBLEM

Consider the two dimensional scattering problem illustrated in Figure 1. In this configuration, the first region is homogeneous with relative dielectric permittivity ε_1 and conductivity σ_1. The second layer has extent equal to d and is homogeneous with relative dielectric permittivity ε_2 and conductivity σ_2. The third region is homogenous with relative dielectric permittivity ε_3 and conductivity σ_3. The complex equivalent relative permittivity in each layer has an explicit dependency on frequency given by:

$$\varepsilon_i^{eq}(\omega) = \varepsilon_i + j\sigma_i/\omega\varepsilon_o, \qquad \textbf{(2.1)}$$

ε_o being the free space dielectric permittivity and ω the pulsation. The magnetic permeability is everywhere equal to that of the free-space, μ_o.

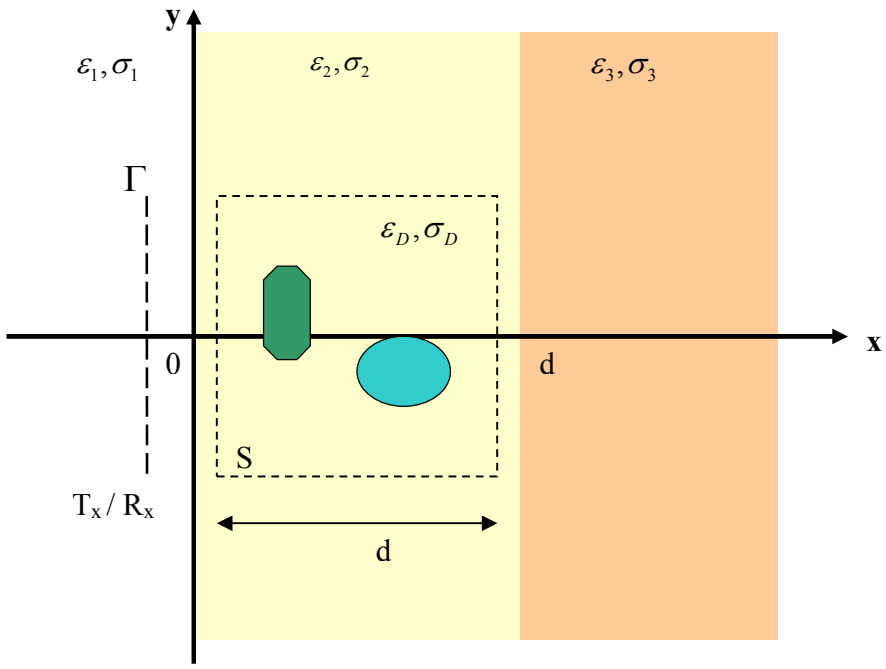

Figure 2.1 – Geometry of the problem

We suppose that infinitely long cylindrical objects having cross sections invariant with respect to the *z*-axis are embedded in the second layer and that their cross sections are contained within an a priori fixed square investigation domain *S,* completely embedded in the second layer. The unknowns of the problem are the spatial distribution of the relative dielectric permittivity ε_D and that of the conductivity σ_D over the investigation domain *S*.

The source of the incident field is a filamentary *z*-directed electric current (TM polarization), of non finite extent and constant along the *z*-axis, which radiates at different frequencies. Such a source is located in the first layer and it is moved along the line Γ parallel to the first interface and located very close to it. In order to collect multifrequency/multiview/multistatic data, for each working frequency and at each position of the source the electric field scattered by the buried targets is measured in several locations along Γ.

Under the above assumptions, the total field in whole space in the absence of the buried objects will be in the form

$$\overline{E}^0 = (\mathbf{r}, \mathbf{r'}) = (0, 0, E^0(\mathbf{r}, \mathbf{r'})) \qquad \textbf{(2.2)}$$

where

$$\mathbf{r} = (x, y) \text{ and } \mathbf{r'} = (x', y') \qquad \textbf{(2.3)}$$

It is worth to remark that such a set-up can be practically realized by using only a pair of antennas. As a matter of fact, exploiting a "synthetic array" strategy, one antenna acts as transmitter and the other one, which acts as receiver, is moved along the measurement line in the desired positions. By repeating this procedure for different locations of the transmitting antenna, one can achieve the desired set of data.

Since the problem is invariant in the z-direction, the total field in the space, say $\overline{E}$, will also be parallel to the Oz-axis which leads to reduce the problem to a scalar one in terms of the wave functions E^0, E and E^s when E^s is the scattered field due to the buried objects. In such a case one can easily show that the scattered field which is defined as

$$E^s = E - E^0 \tag{2.4}$$

satisfies the reduced wave equation

$$\Delta E^s(\mathbf{r},\mathbf{r}') + k^2(x)E^s(\mathbf{r},\mathbf{r}') = -k^2(x)\chi(\mathbf{r})E(\mathbf{r},\mathbf{r}') \tag{2.5}$$

under the boundary conditions and radiation condition at infinity. Here we put

$$k^2(x) = \begin{cases} k_1^2, & x < 0 \\ k_2^2, & x \in (0,d) \\ k_3^2, & d < x \end{cases} \tag{2.6}$$

which is nothing but the square of the wave number of the three-part-space. In (2.6) k_1, k_2 and k_3 are the wave numbers of the media $x < 0$, $x \in (0,d)$ and $d < x$ respectively.

The function $\chi(\mathbf{r})$ appearing in (2.5) is so-called contrast function and is defined as

$$\chi(\omega,\mathbf{r}) = \frac{\varepsilon_D^{eq}(\omega,\mathbf{r})}{\varepsilon_2^{eq}(\omega)} - 1 \tag{2.7}$$

where

$$\varepsilon_D^{eq}(\omega,\mathbf{r}) = \varepsilon_D(\mathbf{r}) + j\sigma_D(\mathbf{r})/(\omega\varepsilon_0) \tag{2.8}$$

From (2.7) and (2.8) one can easily conclude that the function $\chi(\mathbf{r})$ is identically zero outside the objects.

Such a complex function changes with frequency and this does not allow to consider it as the actual unknown in the multifrequency case. However, assuming a priori that ε_D and σ_D in (2.8) are independent of frequency, we can introduce a pair of frequency independent real functions:

$$\Delta\varepsilon = \varepsilon_D - \varepsilon_2, \quad \Delta\sigma = \frac{\sigma_D - \sigma_2}{\omega_m \varepsilon_0} \quad , \tag{2.9}$$

ω_m being the maximum working frequency. These functions are simply related to χ:

$$\chi(\omega,\mathbf{r}) = \frac{1}{\varepsilon_2^{eq}}\left(\Delta\varepsilon(\mathbf{r}) - \frac{j\omega_m}{\omega}\Delta\sigma(\mathbf{r})\right), \tag{2.10}$$

and in what follows we will assume them as the actual unknowns of our inverse problem. By doing so, we are able to deal with frequency independent unknowns, $\Delta\varepsilon$ and $\Delta\sigma$, without neglecting the dispersive nature of the problem.

The transformation of (2.5) into an integral equation through the Green's function of the three-part-space, say $G(\mathbf{r},\mathbf{r}')$, yields a more convenient relation between the contrast function $\chi(\mathbf{r})$ and the scattered field $E^s(\mathbf{r})$. After some straightforward manupulations one gets [19]

$$E^s(\mathbf{r}_\mathbf{r},\mathbf{r}_\mathbf{t},\omega) = k_2^2 \int_D E(\mathbf{r}',\mathbf{r}_\mathbf{t},\omega)\,\chi(\mathbf{r}',\omega)\,G_{21}(\mathbf{r}_\mathbf{r},\mathbf{r}')\,d\mathbf{r}' \tag{2.11}$$

This is the relation which connects the scattered field measured at the observation location $\mathbf{r}_\mathbf{r}$ for the source located at $\mathbf{r}_t$ with the contrast function $\chi(\mathbf{r}',\omega)$ which is called "data equation". Similarly, by rearranging (2.11), and writing the resulting expression for the observation points inside the object, one gets

$$E(\mathbf{r},\mathbf{r}_\mathbf{t},\omega) - E^0(\mathbf{r},\mathbf{r}_\mathbf{t},\omega) = k_2^2 \int_D E(\mathbf{r}',\mathbf{r}_\mathbf{t},\omega)\,\chi(\mathbf{r}',\omega)\,G_{22}(\mathbf{r},\mathbf{r}',\omega)\,d\mathbf{r}' \tag{2.12}$$

which is nothing but so-called "object equation". The functions appearing in (2.11) and (2.12) are the Green's function of the three part space which we will give their explicit expressions below. Thus, the scattering problem is reduced to the solution of coupled system of integral equations given by (2.11) and (2.12). Before going any further, it would be appropriate to give explicit expressions of the Green's function and the total field E^0 in whole space in the absence of the buried objects.

2.1 An Explicit Expression of the Green's Function

By definition, the Green's function $G(\mathbf{r},\mathbf{r}')$ of the three part space satisfies the equation

$$\Delta G + k^2 G = -\delta(\mathbf{r}-\mathbf{r}') \tag{2.13}$$

In the sense of distributions and under radiation condition. In (2.11) and (2.12), we need only its explicit expressions valid for $x<0$ and $x\in(0,d)$, respectively, while $y\in(0,d)$.

First we consider the Fourier transform of $G(x,y;\mathbf{r}')$ with respect to y;

$$\hat{G}(\upsilon,x;\mathbf{r}') = \int G(x,y;\mathbf{r}')e^{-j\upsilon y}dy \tag{2.14}$$

Then (2.13) will become

$$\frac{\partial}{\partial x^2}\hat{G} - \left[\upsilon^2 - k^2(x)\right]\hat{G} = -e^{-j\upsilon y'}\delta(x-x') \tag{2.15}$$

After we solve this differential equation and using the boundary conditions, which are

$$\begin{aligned}
&x=0 \quad \Rightarrow \quad \hat{G}^+ = \hat{G}^- \quad \text{and} \quad \frac{\partial}{\partial x}\hat{G}^+ = \frac{\partial}{\partial x}\hat{G}^- \\
&x=x' \quad \Rightarrow \quad \hat{G}^+ = \hat{G}^- \quad \text{and} \quad \frac{\partial}{\partial x}\hat{G}^+ - \frac{\partial}{\partial x}\hat{G}^- = -e^{-j\upsilon y'} \\
&x=d \quad \Rightarrow \quad \hat{G}^+ = \hat{G}^- \quad \text{and} \quad \frac{\partial}{\partial x}\hat{G}^+ = \frac{\partial}{\partial x}\hat{G}^-
\end{aligned} \tag{2.16}$$

we obtain

$$\hat{G}(\upsilon,x;y) = \begin{cases}
\hat{G}_{11}\ , & x<0, \quad y<0 \\
\hat{G}_{12}\ , & x<0, \quad 0<y<d \\
\hat{G}_{21}\ , & 0<x<d, \quad y<0 \\
\hat{G}_{22}\ , & 0<x<d, \quad 0<y<d
\end{cases} \tag{2.17}$$

where $\upsilon\in C_1$ (Figure 2.2) and

$$\hat{G}_{12} = \frac{e^{-j\upsilon y'}}{2\gamma_2} \frac{T_{12}}{R_{12}R_{32}e^{-2\gamma_2 d} - 1} (e^{\gamma_1 x - \gamma_2 x'} + R_{32}e^{-2\gamma_2 d} e^{\gamma_1 x + \gamma_2 x'}) \tag{2.18}$$

$$\hat{G}_{22} = \frac{e^{-j\upsilon y'}}{2\gamma_2} \frac{\left[R_{12}e^{-\gamma_2(x+x')} + R_{32}e^{-2\gamma_2 d} e^{\gamma_2(x+x')} + (R_{12}R_{32}e^{-2\gamma_2 d} + 1)e^{\gamma_2|x-x'|} \right]}{R_{12}R_{32}e^{-2\gamma_2 d} - 1} \tag{2.19}$$

with

$$T_{12} = \frac{2\gamma_2}{\gamma_2 + \gamma_1}, \qquad R_{12} = \frac{\gamma_2 - \gamma_1}{\gamma_2 + \gamma_1}, \qquad R_{32} = \frac{\gamma_2 - \gamma_3}{\gamma_2 + \gamma_3} \tag{2.20}$$

and

$$\gamma_1 = \sqrt{\upsilon^2 - k_1^2} \ , \qquad \gamma_2 = \sqrt{\upsilon^2 - k_2^2} \ , \qquad \gamma_3 = \sqrt{\upsilon^2 - k_3^2} \tag{2.21}$$

The square-root functions in (2.21) are defined in the complex υ-plane cut as shown in Figure 2.2 such that:

$$\gamma_1 \to -jk_1 \ , \qquad \gamma_2 \to -jk_2 \ , \qquad \gamma_3 \to -jk_3 \ , \qquad \text{as } \upsilon \to 0 \tag{2.22}$$

An explicit expression of $G(\mathbf{r},\mathbf{r}')$ can be obtained through the inverse Fourier transform integral;

$$G(\mathbf{r},\mathbf{r}') = \frac{1}{2\pi} \int_R \hat{G}(\upsilon, x; \mathbf{r}') e^{j\upsilon y'} d\upsilon \tag{2.23}$$

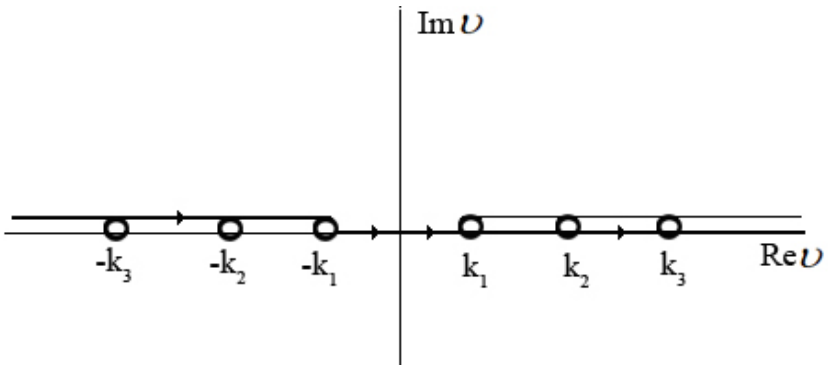

Figure 2.2: Mapping the C_1 in the complex υ-plane

2.2 The Field

By means of the Green-Sommerfield functions it is also possible to evaluate the field E^0 in domain D produced by a filamentary current I_0 located in the first medium at a distance x_t from the interface:

$$E^0(\mathbf{r},\mathbf{r_t}) = \frac{\omega\mu_0 I_0}{2\pi}\int_{-\infty}^{\infty}\frac{e^{j\upsilon(y-y')}}{2\gamma_1}\frac{T_1}{R_1R_3+1}(e^{\gamma_1 x_t-\gamma_2 x}+R_3e^{\gamma_1 x_t+\gamma_2 x})d\upsilon \qquad \textbf{(2.24)}$$

As it can be seen G_{12}, G_{22} and the field E^0 can be interpreted as 1-dimensional Fourier transforms in the spatial frequency υ and therefore can be efficiently computed by means of Fast Fourier Transforms.

Some remarks on the solution of the forward scattering problem can be found in [18].

3. THE LINEARIZED TOMOGRAPHIC APPROACH

In its general formulation, see (2.11-12), the problem we are dealing with is non-linear. However, in some cases it is possible to describe the problem by means of an approximated model. In this section, we will give the details of a linearization procedure under Born Approximation.

3.1 The Born Approximation

The Born approximation [15] consists in neglecting the mutual interactions between the objects and amounts to assume the internal field E in D equal to the unperturbed one E^0. This allows a considerable simplification since the electromagnetic scattering is modeled by means of a single linear integral equation.

When the targets are embedded in a lossy medium, a large number of cases can be modeled by means of the BA [20], since presence of losses smoothes multiple scattering effects. Considering that in masonry diagnostics as well as in subsurface prospecting involved media are usually lossy, we will consider in the following the BA.

In this case, the data equation given by (2.11) will become:

$$E_s\left(\mathbf{r}_\mathbf{r},\mathbf{r}_\mathbf{t},\omega\right)=k_2^2\int_D \frac{E^0\left(\mathbf{r}',\mathbf{r}_\mathbf{t},\omega\right)G_{21}\left(\mathbf{r}_\mathbf{r},\mathbf{r}'\omega\right)}{\varepsilon_2+j\sigma_2/\omega\varepsilon_o}\times\left(\Delta\varepsilon\left(\mathbf{r}'\right)+\frac{j\omega_m}{\omega}\Delta\sigma\left(\mathbf{r}'\right)\right)d\mathbf{r}' \qquad \textbf{(3.1)}$$

and the problem can be cast as the inversion of the linear operator given by (3.1) and defined as:

$$\mathcal{L}_{\mathrm{DB}}: x\in X\subset L^2(D)\times L^2(D)\rightarrow E_s\in Y\subset L^2(\Gamma\times\Gamma\times\Phi). \qquad \textbf{(3.2)}$$

In (3.2) X is a subspace containing all the pairs of functions $x=\left(\Delta\varepsilon,\Delta\sigma\right)$ and the data space Y is a subspace containing the scattered fields corresponding to all possible

measurement positions over Γ, all possible source positions over Γ and to the frequency band Φ.

Due to the properties of its kernel, $\mathcal{L}_{DB}$ is a compact operator, so that its inversion is an ill-posed problem and the necessity of restoring well-posedness arises [7]. Therefore a suitable regularization scheme has to be adopted in order to set up a stable and reliable solution.

3.2 Singular Value Decomposition (SVD)

One of the most fruitful tools in the theory of linear inverse problems is the singular value decomposition (SVD) of a matrix and its extension to certain classes of linear operators. Indeed, SVD is basic both for understanding the ill-posedness of linear inverse problems and for describing the effect of the regularization methods [7].

By means of an arbitrary MxN matrix **A**, with rank $p \le \min\{M, N\}$, it is always possible to form two self-adjoint matrices and precisely

$$\overline{\mathbf{A}} = \mathbf{A}^*\mathbf{A} \ , \ \underline{\mathbf{A}} = \mathbf{A}\mathbf{A}^* \qquad \textbf{(3.3)}$$

The first one is NxN while the second is MxM. They have the following properties:

- both matrices are self-adjoint and positive semi-definite
- both matrices have rank p

[Since both matrices have exactly p positive eigenvalues, the zero eigenvalue has multiplicity N – p for the matrix $\overline{\mathbf{A}}$ and M – p for the matrix $\underline{\mathbf{A}}$. If $M \neq N$, at least one of the two matrices has the zero eigenvalue and precisely the matrix which has the largest dimension.]

The first basic result is the following: the matrices $\overline{\mathbf{A}}$ and $\underline{\mathbf{A}}$ have exactly the same positive eigenvalues with the same multiplicity. The proof of this result is easy. Let us consider the matrix $\overline{\mathbf{A}}$. Since it is symmetric and positive semi-definite, from the properties mentioned above it follows that it has p positive eigenvalues

$\sigma_1^2 \geq \sigma_2^2 \geq ... \geq \sigma_p^2$; we will denote by $v_1, v_2, ..., v_p$ the eigenvectors associated with these eigenvalues. These eigenvectors form an orthonormal basis in the orthogonal complement of the null space of the matrix $\mathbf{A}$, $\mathcal{N}(\mathbf{A})$. To each eigenvector v_k, which is a vector of ε_N, we can associate a vector of ε_M as follows

$$u_k = \frac{1}{\sigma_k}\mathbf{A}v_k \tag{3.4}$$

All vectors u_k are different from zero and they are eigenvectors of $\overline{\mathbf{A}}$ associated with the eigenvalue σ_k^2. Indeed

$$\overline{\mathbf{A}}u_k = \mathbf{A}\mathbf{A}^* u_k = \frac{1}{\sigma_k}(\mathbf{A}\mathbf{A}^*)\mathbf{A}v_k = \frac{1}{\sigma_k}\mathbf{A}(\mathbf{A}^*\mathbf{A})v_k = \frac{1}{\sigma_k}\mathbf{A}(\sigma_k^2 v_k) = \sigma_k^2 u_k \tag{3.5}$$

This simple computation implies that all positive eigenvalues of $\overline{\mathbf{A}}$ are also positive eigenvalues of $\mathbf{A}$. If all σ_k^2 have multiplicity one, the two matrices have precisely the same eigenvalues because also $\mathbf{A}$ can have only *p* positive eigenvalues. The proof is not complete in the case of eigenvalues with multiplicity > 1. However, if we compute the scalar products of the vectors u_k, we obtain

$$(u_k . u_j)_M = \frac{1}{\sigma_k \sigma_j}(\mathbf{A}v_k . \mathbf{A}v_j)_M = \frac{1}{\sigma_k \sigma_j}(\mathbf{A}^*\mathbf{A}v_k . v_j)_N = \frac{\sigma_k}{\sigma_j}(v_k . v_j)_N = \delta_{k,j}, \tag{3.6}$$

Where we have indicated with a suffix the dimension of the space. This result implies that the eigenvectors u_k are orthonormal, so that they are linearly independent even when they are associated with the same positive eigenvalue. Since we have obtained *p* linearly independent eigenvectors and since $\mathbf{A}$ has precisely *p* linearly independent eigenvectors associated with positive eigenvalues, we have proved that equation (3.4) provides all these eigenvectors of $\mathbf{A}$. This remark completes the proof of the result stated above.

If we multiply by $\mathbf{A}^*$ both sides of equation (3.4) we obtain

$$\frac{1}{\sigma_k}\mathbf{A}^* u_k = \frac{1}{\sigma_k^2}\mathbf{A}\mathbf{A}^* v_k = v_k \tag{3.7}$$

Therefore equations (3.4) and (3.7) show that the eigenvectors u_k, v_k are solution of the following *shifted eigenvalue problem,*

$$\mathbf{A}v_k = \sigma_k u_k, \qquad \mathbf{A}^* u_k = \sigma_k v_k \tag{3.8}$$

The positive numbers σ_k are called the *singular values,* the vectors u_k, v_k are called the *singular vectors,* and the triplet $\{\sigma_k, u_k, v_k\}_{k=1}^{\infty}$ is called the *singular system* of the matrix $\mathbf{A}$. Then the *singular value decomposition* of the matrix $\mathbf{A}$ would be:

$$\mathbf{A} = u_k \sigma_k v_k \tag{3.9}$$

We can provide a regularized inversion for (3.1) by the SVD of the operator $\mathcal{L}_{\mathrm{DB}}$ in (3.2), which defines a triplet $\{\sigma_n, u_n, v_n\}_{n=1}^{\infty}$ such that:

$$\mathcal{L}_{\mathrm{DB}}(u_n) = \sigma_n v_n, \quad \mathcal{L}_{\mathrm{DB}}^{+}(v_n) = \sigma_n u_n \tag{3.10}$$

wherein $\mathcal{L}_{\mathrm{DB}}^{+}$ is the adjoint operator of $\mathcal{L}_{\mathrm{DB}}$, $\{\sigma_n\}_{n=1}^{\infty}$ denotes the sequence of the singular values ordered in non increasing sequence and u_n and v_n form the basis for the space of the visible objects (that is the objects which can be recovered by the error-free data) and for the closure of the range (that is the space of the noise-free data) of the operator, respectively.

Exploiting the SVD of the relevant operator, the formal solution of integral equation (3.1) can be cast as:

$$x = \sum_{n=1}^{\infty} \frac{1}{\sigma_n} < E_s, v_n > u_n \tag{3.11}$$

where <.,.> denotes the scalar product in data space.

The compactness of $\mathcal{L}_{DB}$ entails that the sequence of the singular values asymptotically decays to zero [7]. Therefore ill-posedness of the inverse problem given by (3.1) immediately appears: indeed, in presence of noise on data, the contributions to the solution related to the singular values closer to zero will be strongly corrupted by noise and the result of the inversion will become unstable.

A simple way to tackle such an instability consists in truncating the expansion (3.11) to those terms that are not overwhelmed by noise. Therefore we assume as a regularized solution of our problem the one obtained by means of the Truncated SVD expansion:

$$x = \sum_{n=1}^{N} \frac{1}{\sigma_n} < E_s, v_n > u_n . \qquad \textbf{(3.12)}$$

By restricting the solution space to that spanned by the first N singular functions, this regularized solution is stable with respect to errors on data. However, since it is achieved by considering only a reduced number of terms in (3.11) this procedure will lead to an approximate representation of the sought unknown. Therefore, the choice of the index N represents a trade-off between the accuracy of the solution and its stability with respect to noise. Such an optimal choice, in its turn, is actually related to the estimated level of noise and to the model error[1]. As a consequence, the optimal choice may be a chimera, because the model error depends on the unknown scattering object. Lacking definite criteria to determine such an optimal choice, we have chosen in our regularized approach to reject the contributions related to singular values 20 dB lower than the maximum one.

3.3 The Discretization Procedure

The numerical implementation of the inversion procedure described above is based on an equivalent matrix formulation of the problem in which only real vectors are involved.

As a first step to implement one has to discretize the unknown parameters within the investigation domain D. In order to certainly satisfy the criteria outlined in [21], the pair

[1] The model error is the discrepancy between the actual scattered field data and those that would result according to the BA.

of unknown functions is expanded by using as a basis the pulse functions defined within N_cxN_c square cells whose side is $\lambda/20$ long, λ being the minimum wavelength, thus rendering the results of the discretized version of the problem very close to those of the continuous problem in (3.1). The vector of the unknowns is now defined as a column vector of dimension $2N_c^2$, whose first N_c^2 rows contain $\Delta\varepsilon$, and the second N_c^2 rows contain $\Delta\sigma$.

A discrete set of measurements N_m, incident fields N_v and frequencies N_f is considered, leading to $M = N_m$xN_vxN_f complex data. Therefore, the data vector is defined as a column vector of dimension $2M$, in which the real part of the scattered fields (considered at each frequency, incident field and measurement point) is stored in the first M rows, and the imaginary part is stored in the latter M rows.

By following this procedure one achieves the matrix equation:

$$\begin{bmatrix} \mathbf{A} & \mathbf{B} \\ \mathbf{C} & \mathbf{D} \end{bmatrix} \cdot \begin{bmatrix} \Delta\varepsilon \\ \Delta\sigma \end{bmatrix} = \begin{bmatrix} Re(E_S) \\ Im(E_S) \end{bmatrix}, \qquad \textbf{(3.13)}$$

wherein **A**, **B**, **C**, **D** are block matrices of dimension MxN_c^2, computed by separating the discretized counterpart of (3.1) in its real and imaginary parts.

The discretized problem, as stated in (3.3), can be now solved by means of the numerical SVD applied to real matrices.

4. NUMERICAL RESULTS

In this section we will give some examples aimed at showing the reconstruction capabilities of the considered inversion approach, and also at discussing how it can be used as a tool to fix the measurement set-up. The reference situation is the one depicted in Figure 2.1. It is supposed that transmitting and receiving antennas are uniformly spaced over the observation domain Γ. In addition, as suggested by the arguments in [16], it is convenient to assume that the number of transmitters and receivers locations is the same. In this way it results N_v=N_m, that is for each of the N_m positions of the transmitter, N_m measurement are collected (multiview / multistatic configuration).

4.1 Case 1 : Investigating The Effect Of The Slab

As a general comment one can notice that the presence of the second interface in Figure 2.1 brings multiple interactions, so that, as a consequence, one can expecct that this makes it more difficult for the linear model to work reliably. That is because, during the linearization of the model performed with the Born Approximation, multiple interactions are actually neglected. On the other hand, if the amount of losses in the second medium grows, then it is expected that these interactions would fade away, so that the negative effect of the second interface would be overcome.

As a first example we consider a situation in which the relative dielectric permittivities of the second medium, the third medium and the target were selected as 4, 3.95 and 4.1 respectively, and the conductivities were selected equal and 0.001 S/m. Therefore since the relative permittivities of the medium 2 and medium 3 are very close to each other, the multiple interactions due to the presence of the discontinuity would be very small. In this situation, we have then applied the linearized inversion using a single frequency of 200 MHz, and 11 transmitting and 11 receiving antennas. As it can be observed from Figure 4.1a, the result appears to be quite poor due to the very small amount of adopted

data. Nevertheless, the inversion algorithm can detect the presence of the target and its horizontal extent**.**

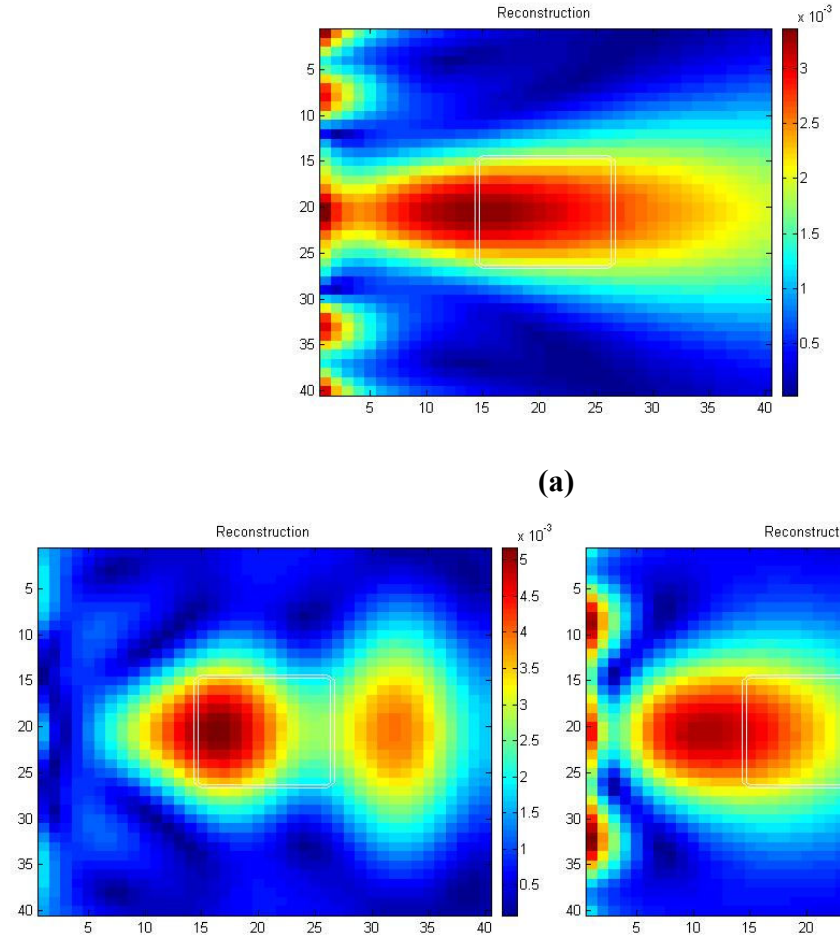

(a)

(b) **(c)**

Figure 4.1: $f = 200$MHz, 11Tx, 11Rx, $\varepsilon_2 = 4$, $\varepsilon_D = 4.1$ **(a)** $\sigma_2, \sigma_3, \sigma_D = 0.001$ S/m, $\varepsilon_3 = 3.95$, **(b)** $\sigma_2, \sigma_D = 0.001$ S/m, $\sigma_3 = 0$, $\varepsilon_3 = 1$ **(c)** $\sigma_2, \sigma_D = 0.01$ S/m, $\varepsilon_3 = 1$, $\sigma_3 = 0$

As a second example, using the same frequency and the same number of antennas as above, we have changed the parameters of the third medium to the ones of the free space. The interactions which are expected to appear due to the second interface brought a second spot in the reconstruction in Figure 4.1b.

Finally, we have increased the conductivity of the second medium and the target to 0.01 S/m, so that the fading waves would overcome the effect of the interactions. Using the

same frequency and the same number of antennas as above we obtain the reconstruction given in Figure 4.1c. In this case, the presence of larger losses in the second medium gives back a more clear picture of the investigated scenario as most of the multiple interactions are actually not present into the data as they are damped. On the other hand, we can notice that the depth of the target (corresponding to the peak of the red spot) is mispositioned, being located at a shallower depth than the truth. This effect is due to the presence of a larger amount of losses in the target. This feature, which is of course neglected in the adopted linear model, entails a change in the wave propagation inside the target area which is not account for into the model, resulting in the observed error in the position of the reconstruction.

4.2 Case 2 : Low Dielectric Contrast

In the second case, we have considered a rectangular object having a relative permittivity of 4.1 embedded in a medium having a relative permittivity of 4. Their conductivities are both assumed to be 0.001 S/m, and the first and the third media are assumed to be free space. In Figure ex01_03 and ex01_04, the reconstructions of the clear and the noise corrupted data (SNR=30dB) can be seen when a single frequency of 200 MHz is used with 11 transmitting and 11 receiving antennas.

As it can be seen in the figure (Figure 4.2 a-b), using a single and low frequency, the object can be detected and its horizontal dimension can be estimated. However, the size and the location where the object starts and ends are not understandable, and also the noise on the data corrupts the reconstruction, but leaves its main features unaltered. Hence, the regularization achieved via truncation of the SVD is robust.

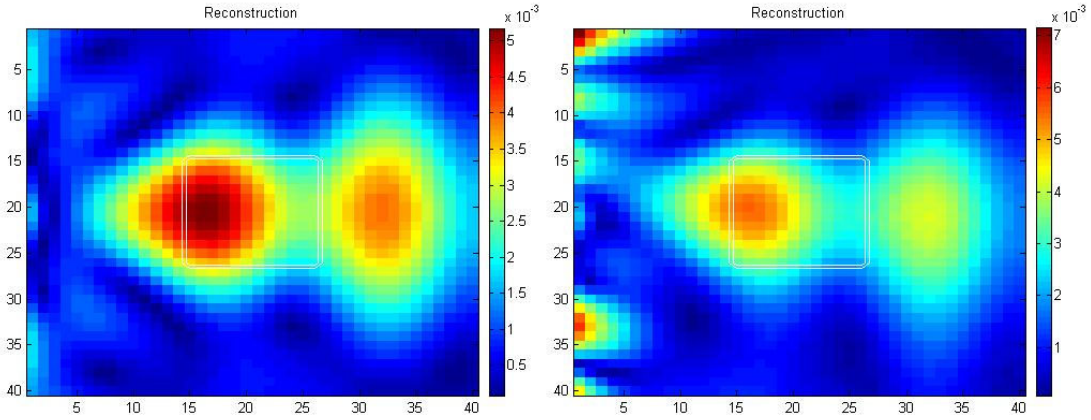

(a) **(b)**

Figure 4.2: $f = 200$ MHz, 11Tx, 11Rx, $\sigma_2, \sigma_D = 0.001\ S/m$, $\sigma_3 = 0$, $\varepsilon_2 = 4$, $\varepsilon_D = 4.1$, $\varepsilon_3 = 1$ **(a)** clear data, **(b)** noise corrupted data

In order to overcome these obstacles, multi-frequency (MF) data can be considered. A useful way to be sure that MF data can be helpful to improve the reconstruction is observing if and how the behaviour of the singular values of the operator pertaining to the multifrequency case differs from that of the single frequency (SF) one (Figure 4.3). In particular, if the number of the singular values larger than the given threshold increases, we can expect that the use of MF will improve the reconstruction. As it can be seen from Figure 4.3, by considering the MF operator, using 200 MHz, 300 MHz and 400 MHz, the number of the above threshold singular values is indeed remarkably larger when using more frequencies, so that we can expect that the reconstruction will improve with respect to that of Figure 4.2.

As it can be observed from Figure 4.4 a-b, using MF data it is possible to locate the target and detect its size better, but a replica appears which may be due to the presence of the second interface or the fact that we do not have enough data.

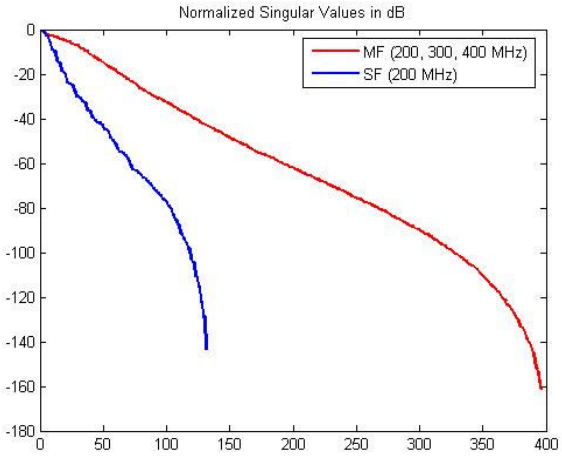

Figure 4.3: Normalized Singular Values for SF and MF case for three frequencies when there is a low dielectric contrast

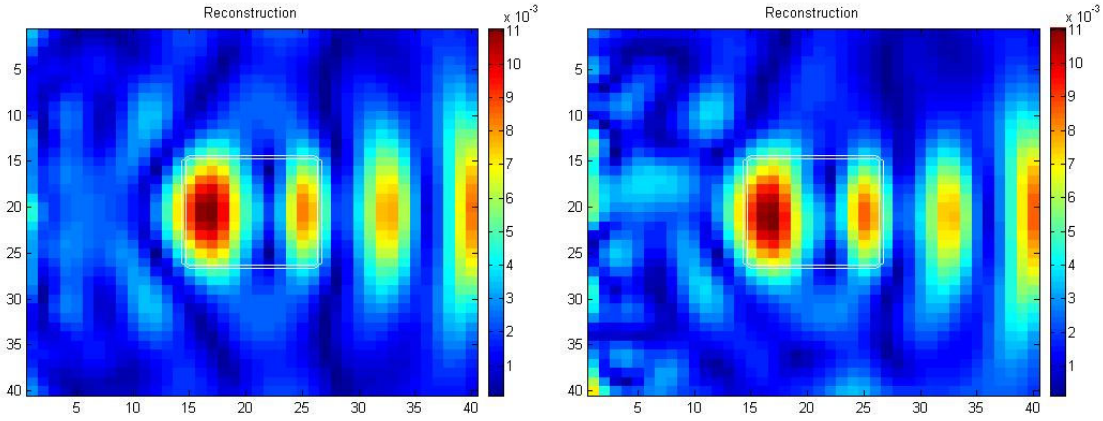

(a) **(b)**

Figure 4.4: $f = 200, 300, 400$ MHz , 11Tx, 11Rx, $\sigma_2, \sigma_D = 0.001\ S/m$, $\sigma_3 = 0$, $\varepsilon_2 = 4$, $\varepsilon_D = 4.1$, $\varepsilon_3 = 1$ **(a)** clear data, **(b)** noise corrupted data

For further improvement, more frequencies in the same frequency band can be considered. In this case, the change in the number of the singular values is very small until -60 dB. That is why a similar reconstruction is expected. (Figure 4.6 a-b)

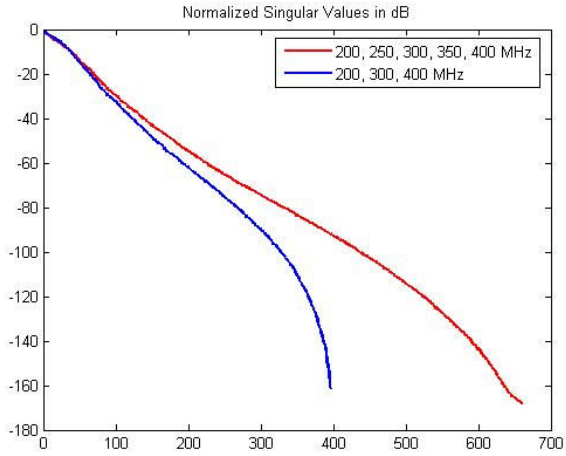

Figure 4.5: Normalized Singular Values for MF cases of three and five frequencies when there is a low dielectric contrast.

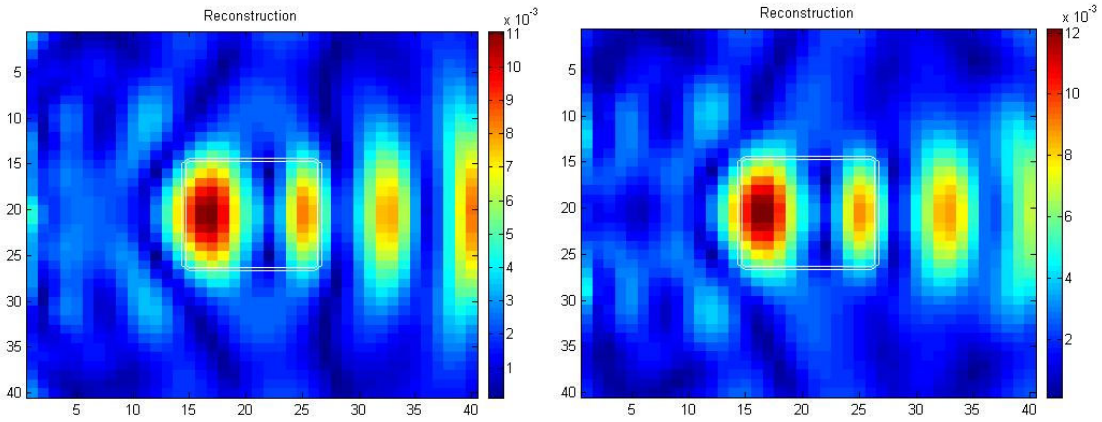

(a) **(b)**

Figure 4.6: $f = 200,\ 250,\ 300,\ 350,\ 400$ MHz , 11Tx, 11Rx, $\sigma_2, \sigma_D = 0.001\ S/m$, $\sigma_3 = 0$, $\varepsilon_2 = 4$, $\varepsilon_D = 4.1$, $\varepsilon_3 = 1$ **(a)** clear data, **(b)** noise corrupted data

Also, one can expect that when the number of transmitters and receivers increases, some independent information about the unknown is added and so the number N of useful singular values to be retained in (3.2.10) increases. However, since the available information about the scattered field is finite, it is expected that a maximum number of antennas exists beyond which the addition of further antennas does not chaange in a significant way the number of useful singular values to be employed in the reconstruction. This can be seen in the figures 4.7, and 4.8 a-b.

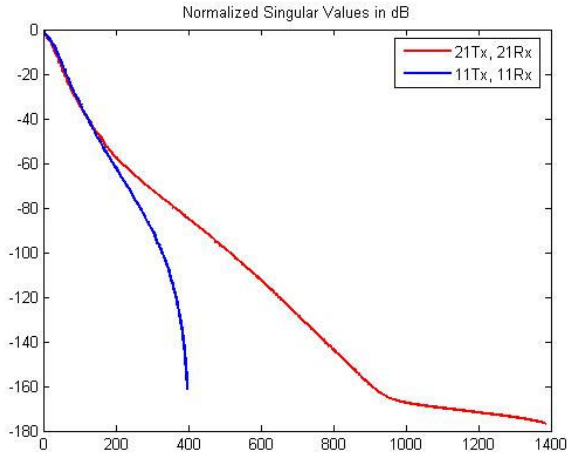

Figure 4.7: Change in the number of Singular Values depending on the number of antennas

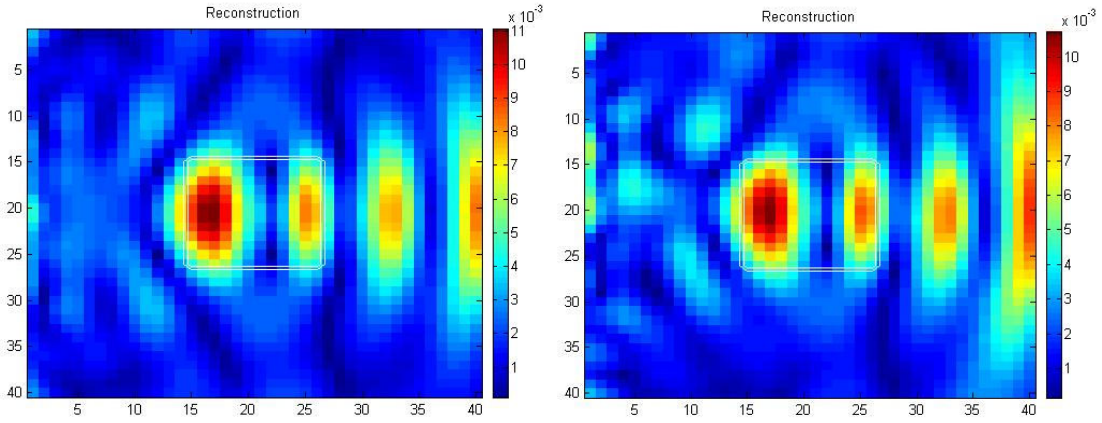

(a) **(b)**

Figure 4.8: $f = 200, 300, 400$ MHz , 21Tx, 21Rx, $\sigma_2, \sigma_D = 0.001\ S/m$, $\sigma_3 = 0$, $\varepsilon_2 = 4$, $\varepsilon_D = 4.1$, $\varepsilon_3 = 1$ **(a)** clear data, **(b)** noise corrupted data

4.3 Case 3 : High Dielectric Contrast

In this example, a rectangular void is placed in a medium having a relative permittivity of 6. The conductivity of the second medium is 0.001 S/m. The first and third media are assumed to be free space. In Figure 4.9 a-b, the reconstructions of the clear and the noise corrupted data (SNR=10) can be seen when a single frequency of 200 MHz is used.

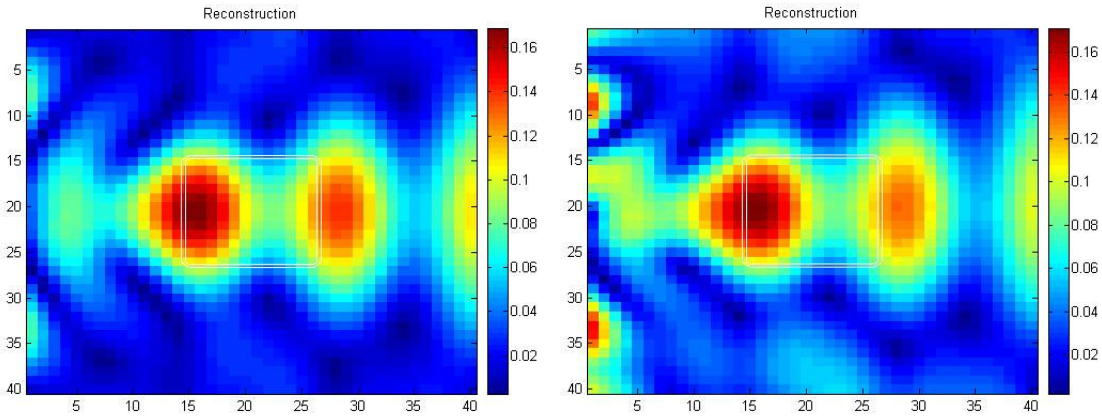

(a) **(b)**

Figure 4.9: $f = 200$ MHz, 11Tx, 11Rx, $\sigma_2 = 0.001\ S/m$, $\sigma_3, \sigma_D = 0$, $\varepsilon_2 = 6$, $\varepsilon_D, \varepsilon_3 = 1$, **(a)** clear data, **(b)** noise corrupted data

Although the contrast between the medium and the target is too high for the Born Approximation, as it can be seen in the figure 4.9 a-b, using a single and low frequency, the object can still be detected and its horizontal dimension can be estimated. However, the size and the location where the object starts and ends are not clearly understandable, and also "ghosts" appear in the deeper part of the investigated region. Moreover, it can be observed that the noise on the data corrupts the reconstruction, but leaves its main features unaltered, thus confirmin that the regularization achieved via truncation of the SVD is robust against uncertainties on data.

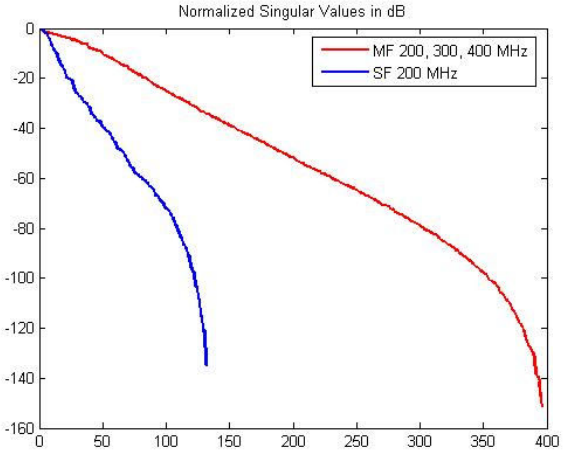

Figure 4.10: Normalized Singular Values for SF and MF case for three frequencies when there is a high dielectric contrast

In order to improve the reconstruction we then consider the use of MF data. Similar to the Case 2, if the number of the singular values for the SF and MF data are observed, as it can be seen in the figure 4.10, the number of the above threshold singular values increase when using more frequencies, so that a better reconstruction is expected.

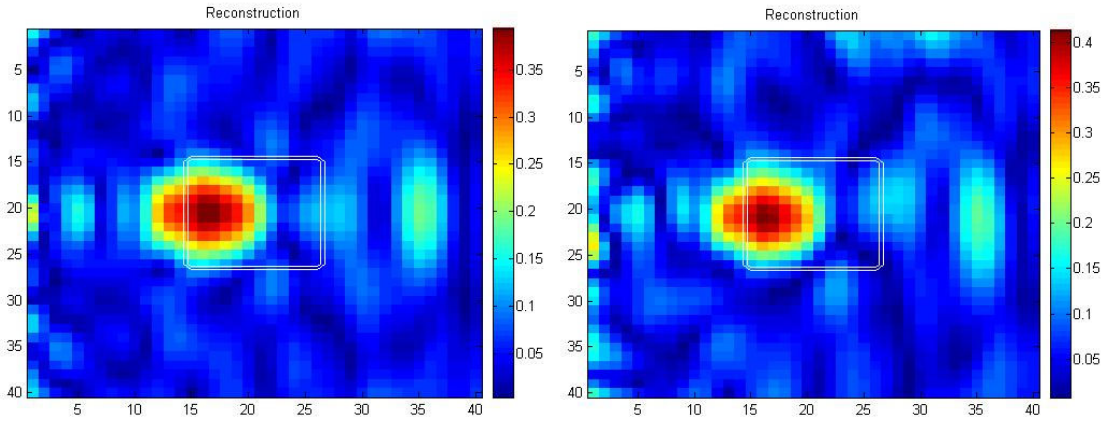

(a) **(b)**

Figure 4.11: $f = 200, 300, 400$ MHz, 11Tx, 11Rx, $\sigma_2 = 0.001\ S/m$, $\sigma_3, \sigma_D = 0$, $\varepsilon_2 = 6$, $\varepsilon_D, \varepsilon_3 = 1$, **(a)** clear data, **(b)** noise corrupted data

Figure 4.11 shows the clean and noisy reconstruction when using MF data. As it can be seen, in both cases, it is possible to accurately locate the target, as the ghosts in the deep part of the investigated region has been filtered out from the reconstruction algorithm and determine its horizontal extent. On the other hand, the vertical dimension of the object cannot be determined as it is not apparent where it ends. This last phenomenon is due to the high contrast of the object, as the effect of the backside of the target is mostly related to multiple interactions which, by definition, are neglected in the adopted linear model.

4.4 Case 4 : Low Conductivity Contrast

In a medium having a relative permittivity of 4 and conductivity 0.001 S/m, an object with the same permittivity but a slightly different conductivity 0.002 has been placed. The first and third media are assumed to be free space. In Figure 4.12 a-b, the

reconstructions of the clear and the noise corrupted data (SNR=30 dB) can be seen when a single frequency of 200 MHz is used.

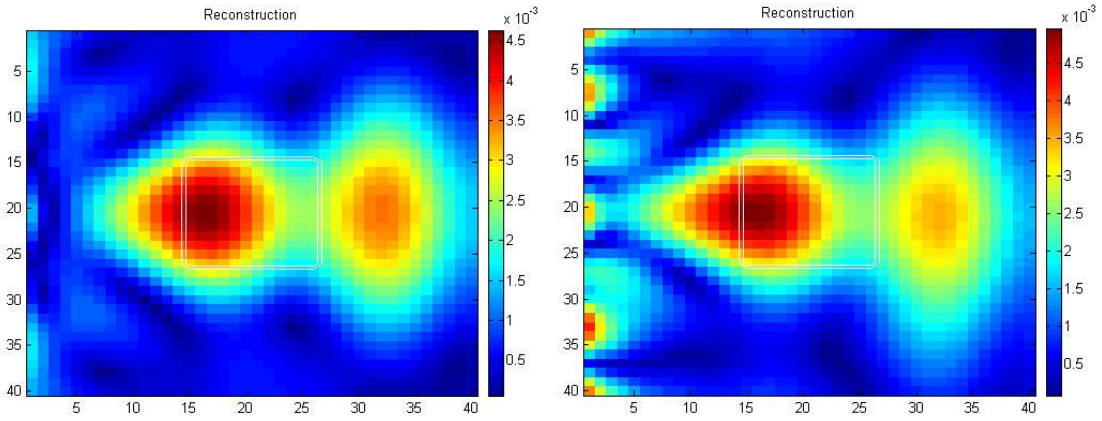

(a) **(b)**

Figure 4.12: $f = 200$ MHz, 11Tx, 11Rx, $\sigma_2 = 0.001\ S/m$, $\sigma_D = 0.002\ S/m$ $\sigma_3 = 0$, $\varepsilon_2, \varepsilon_D = 4$, $\varepsilon_3 = 1$, **(a)** clear data, **(b)** noise corrupted data

Similar to the Case 2, using a single and low frequency, the object can be detected and its horizontal dimension can be estimated. However, the size and the location where the object starts and ends are not understandable, and also the noise on the data, that clearly corrupts the reconstruction, leaves its main features unchanged.

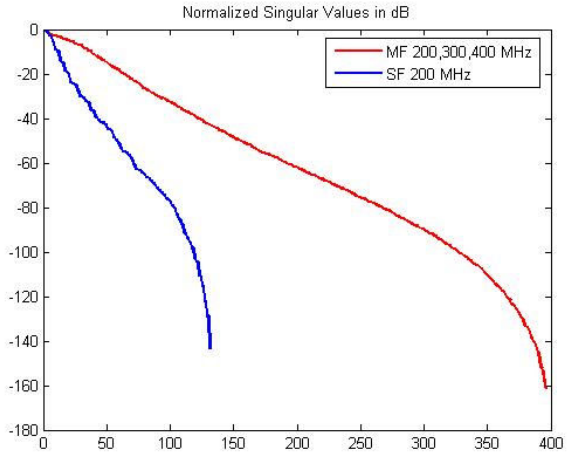

Figure 4.13: Normalized Singular Values for SF and MF case for three frequencies when there is a low conductivity contrast

Similar to the previous cases, if the number of the singular values for the SF and MF data are observed, as it can be seen in the figure 4.13, the number of the above threshold singular values increase when using more frequencies, so that a better reconstruction is expected. This is confirmed in Figure 4.14 a-b.

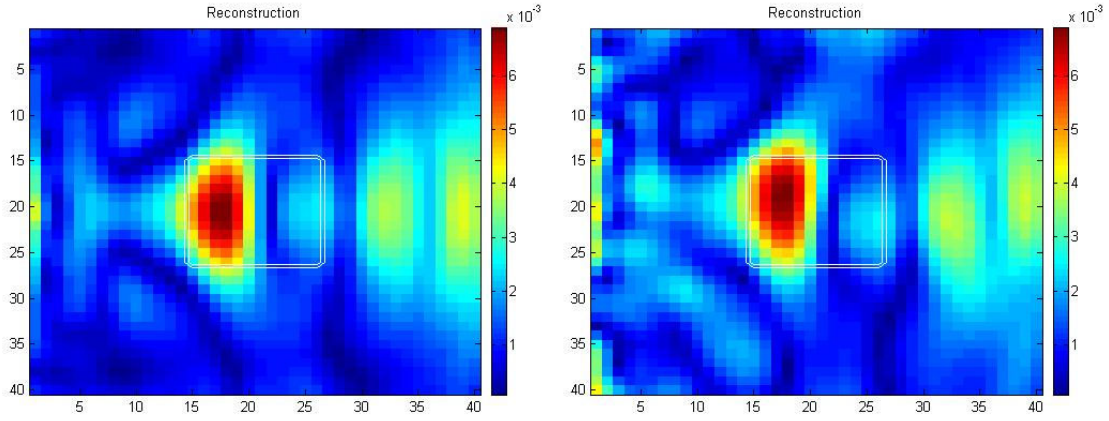

(a) **(b)**

Figure 4.14: $f = 200,\ 300,\ 400$ MHz , 11Tx, 11Rx, $\sigma_2 = 0.001\ S/m$, $\sigma_D = 0.002\ S/m$ $\sigma_3 = 0$, $\varepsilon_2, \varepsilon_D = 4$, $\varepsilon_3 = 1$, **(a)** clear data, **(b)** noise corrupted data

Using MF data (Figure 4.14 a-b) it is possible to locate the target, but although it can be seen where the object starts, its size is not apparent. Again, similar comments as in the previous examples apply.

4.5 Case 5 : High Conductivity Contrast

A rectangular object of a conductivity of 0.9 S/m is placed in a medium whose conductivity is 0.001 S/m. Their relative dielectric permittivities are the same and equal to 4. The first and third media are assumed to be free space. In Figure ex04_01 and ex04_02, the reconstructions of the clear and the noise corrupted data (SNR=20 dB) can be seen when a single frequency of 200 MHz is used.

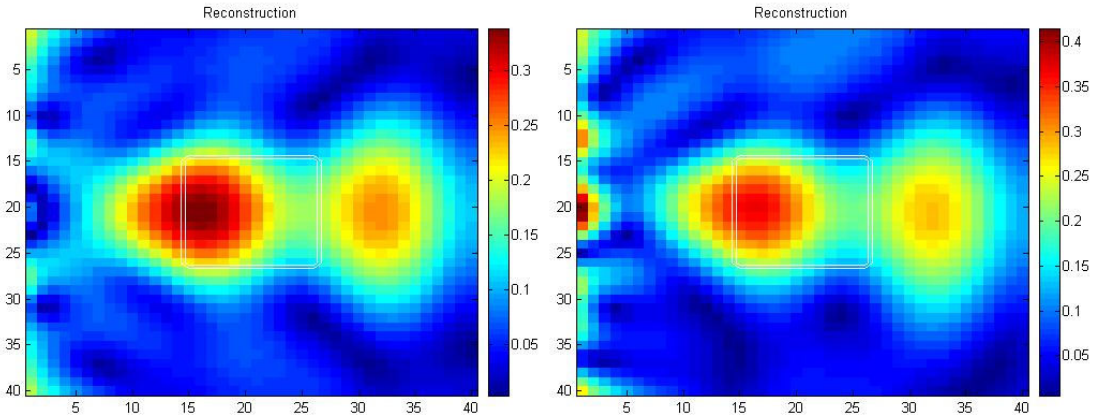

(a) **(b)**

Figure 4.15: $f = 200$ MHz, 11Tx, 11Rx, $\sigma_2 = 0.001\ S/m$, $\sigma_D = 0.9\ S/m$ $\sigma_3 = 0$, $\varepsilon_2, \varepsilon_D = 4$, $\varepsilon_3 = 1$, **(a)** clear data, **(b)** noise corrupted data

Similar to the Case 3, although the contrast between the medium and the target is too high for the Born Approximation, as it can be seen in the Figure 4.15 a-b, using a single and low frequency, the object can still be detected and its horizontal dimension can be estimated. However, the size and the location where the object starts and ends are not understandable, and also the effect of noise is filtered from the regularization procedure in a satisfying way.

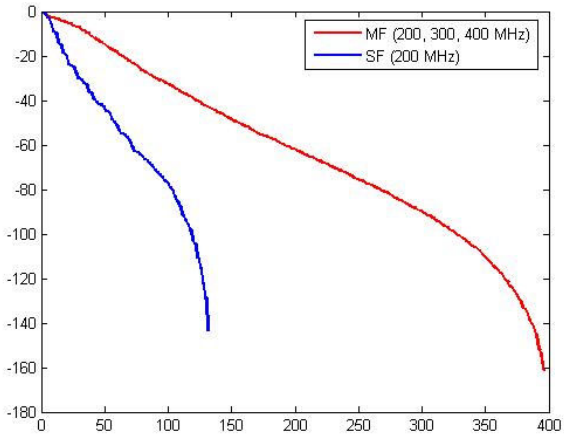

Figure 4.16: Normalized Singular Values for SF and MF case for three frequencies when there is a high conductivity contrast

Similar to the previous cases, if the number of the singular values for the SF and MF data are observed, as it can be seen in the figure 4.16, the number of the above threshold singular values increase when using more frequencies, so that a better reconstruction is expected.

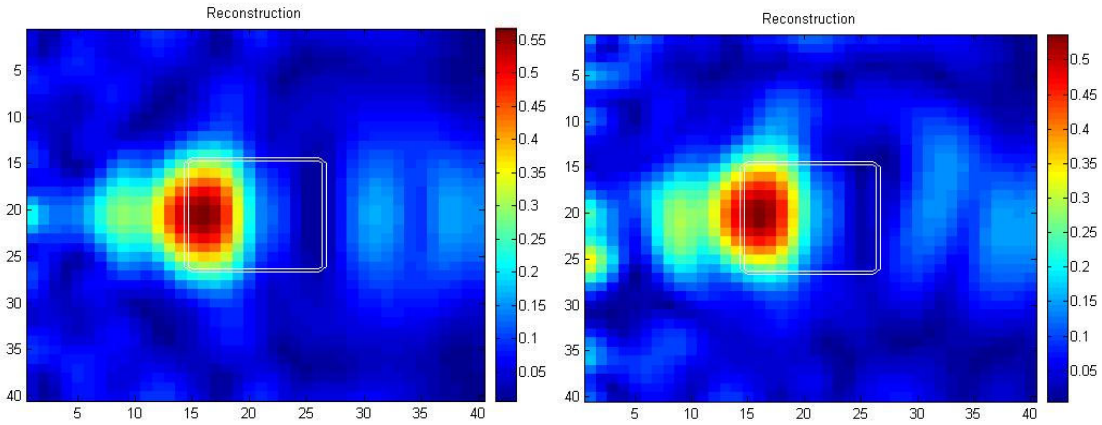

(a) **(b)**

Figure 4.17: $f = 200,\ 300,\ 400$ MHz , 11Tx, 11Rx, $\sigma_2 = 0.001\ S/m$, $\sigma_D = 0.9\ S/m$ $\sigma_3 = 0$, $\varepsilon_2, \varepsilon_D = 4$, $\varepsilon_3 = 1$, **(a)** clear data, **(b)** noise corrupted data

Indeed, using MF data (Figure 4.17) it is then again possible to locate the target, but although it can be seen where the object starts, its size is not apparent.

4.6 Case 6 : Two Objects With Different Dielectric Permittivities

In the sixth example, two objects having relative dielectric permittivities slightly different from each other and also the second medium are used. The second medium, and the objects have relative permittivities of 4, 4.05 and 4.1 respectively, and their conductivities are the same and 0.001.

The first reconstruction was made under the same circumstances as the previous cases with a single and low frequency of 200 MHz. However, although the object which has slightly bigger contrast is detected, the other object is almost invisible (Figure 4.18), and the reconstruction of the detected object is not better than the previous SF cases.

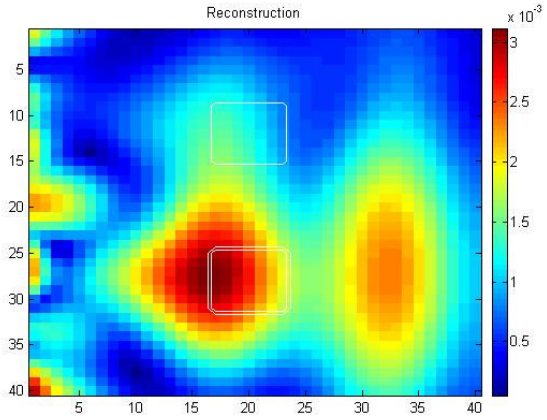

Figure 4.18: $f = 200$ MHz, 1m array, 11Tx, 11Rx, $\sigma_2, \sigma_D = 0.001\ S/m$, $\sigma_3 = 0$, $\varepsilon_2 = 4$, $\varepsilon_{D1} = 4.05$, $\varepsilon_{D2} = 4.1$ $\varepsilon_3 = 1$

In order to improve the reconstruction, using more transmitting and receiving antennas is considered. If the line on which the antennas are placed has the same size, then although the number of antennas increase, a limitation of the information which is caused by the size of the line will stay. That is why, for further improvement in the reconstruction, increasing the length of the line can be considered.

In Figure 4.19, the change in the number of the singular values for different number of antennas and for different length of array is shown. In this figure, it can be seen that an extra number of antennas along the same size of array does not bring an important change of singular values until -60 dB. That is why a similar reconstruction is expected in this case (Figure 4.20 a). On the other hand, if the new number of antennas are placed on a longer array, the number of the singular values apparently increase, that is why an improvement in the reconstruction is expected (Figure 4.20 b).

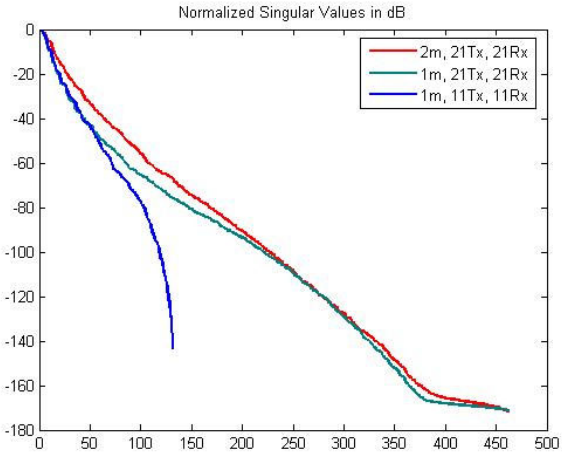

Figure 4.19: Normalized Singular Values depending on the number of the antennas and the length of the array

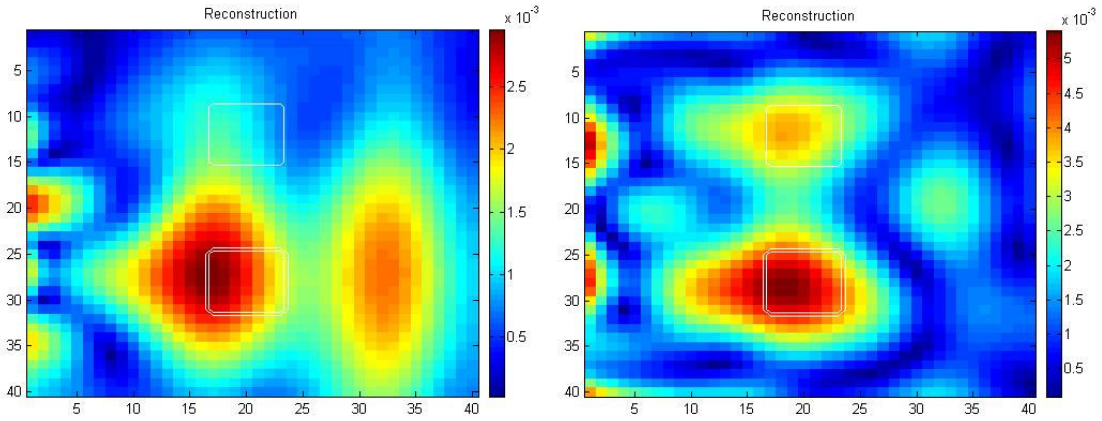

(a) **(b)**

Figure 4.20: $f = 200$ MHz, $\sigma_2, \sigma_D = 0.001\ S/m$, $\sigma_3 = 0$, $\varepsilon_2 = 4$, $\varepsilon_{D1} = 4.05$, $\varepsilon_{D2} = 4.1$ $\varepsilon_3 = 1$, **(a)** 1m array, 21Tx, 21Rx **(b)** 2m array, 21Tx, 21Rx

However, although it is now possible to detect both of the objects in the last reconstruction, it still needs to be improved as many false target appears. Interestingly, the different contrast between the two targets can be inferred from the different values of the magnitude of the reconstructed contrast. This improvement can be done using more frequencies as discussed in previous cases.

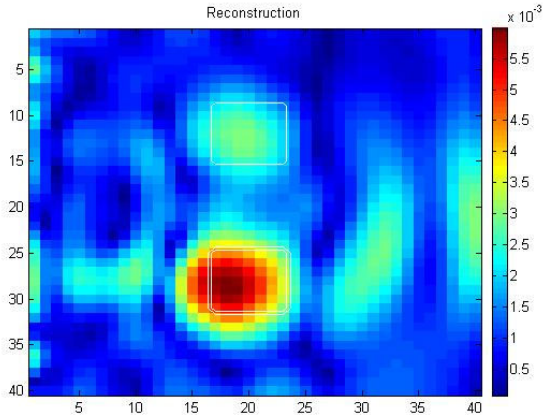

Figure 4.21: $f = 200, 300, 400$ MHz , 1m array, 11Tx, 11Rx, $\sigma_2, \sigma_D = 0.001\ S/m$, $\sigma_3 = 0$, $\varepsilon_2 = 4$, $\varepsilon_{D1} = 4.05$, $\varepsilon_{D2} = 4.1$ $\varepsilon_3 = 1$

The above reconstruction (Figure 4.21) has been made using MF data, it can be seen that the effect of MF is much better than the SF with more antennas and a longer array. However, the object with a smaller contrast is still unclear aand the replica can be mistaken for an object.

The change in the number of the singular values can be seen in Figure 4.22 when more antennas are added and the length of the array is increased. Just like the previous example, we notice that using more antennas along the same sized array (Figure 4.23 a) does not bring results better than the original MF example (Figure 4.21). On the other hand, when the length of the array is increased, a much better reconstruction is obtained (Figure 4.23 b) as the reduction of the false objects due to the larger amount of data, leads to an image in which the two target can be clearly identified, also their different contrast can also be inferred.

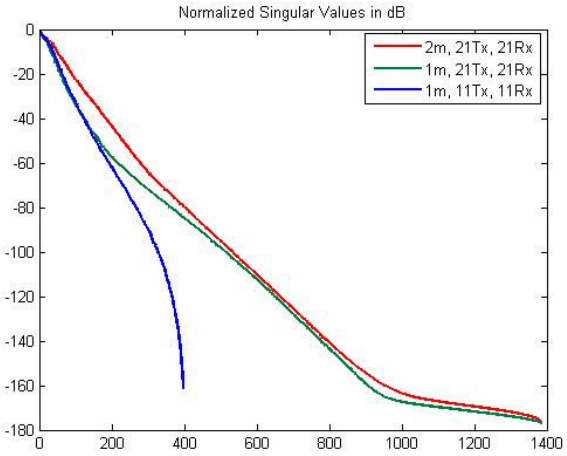

Figure 4.22: Normalized Singular Values depending on the number of the antennas and the length of the array

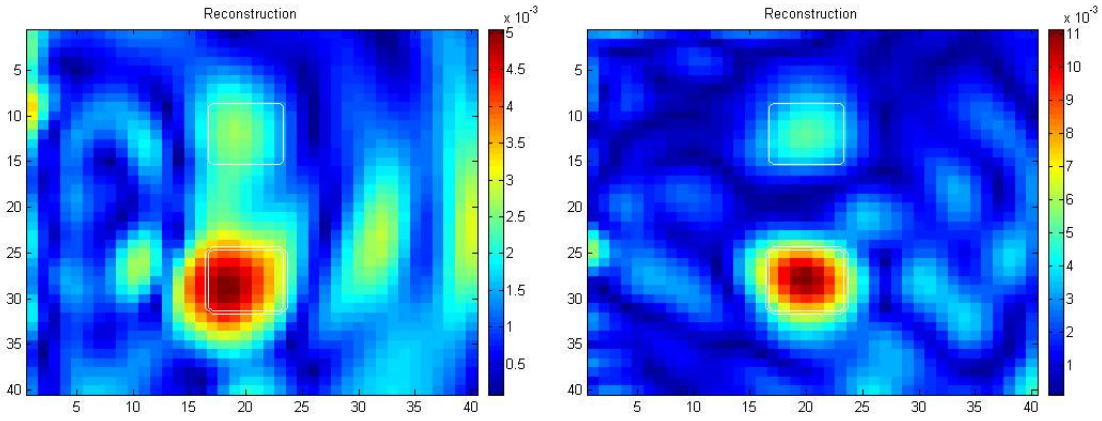

(a) **(b)**

Figure 4.23: $f = 200, 300, 400$ MHz , $\sigma_2, \sigma_D = 0.001\ S/m$, $\sigma_3 = 0$, $\varepsilon_2 = 4$, $\varepsilon_{D1} = 4.05$, $\varepsilon_{D2} = 4.1$ $\varepsilon_3 = 1$, **(a)** 1m array, 21Tx, 21Rx **(b)** 2m array, 21Tx, 21Rx

5. CONCLUSION

A linearized approach elaborated within the framework of the BA for the reconstruction of objects embedded in a layered medium has been presented. A suitable formulation of the problem has allowed to tackle the dispersive nature of the scattering problem considering a pair of frequency independent unknowns, $\Delta\varepsilon$ and $\Delta\sigma$. This allows to exploit multifrequency data at best.

As shown by several numerical examples, the considered approach allows to set up an efficient and reliable solution algorithm. In particular, the regularization strategy proves to be very stable since results obtained with "clean" and noise-corrupted data are almost coincident. Moreover, although the assumptions underlying the BA model actually limit the class of retrievable functions (in terms of the permittivity and the extension of the target with respect to that of the background as well as in terms of its spatial variability), the numerical examples show that the approach can provide good (qualitative) results also in cases in which the linear approximation fails.

The SVD tool has been widely exploited in this thesis not only to set-up to regularize the inverse problem, but also to determine which is the optimal measurement set-up. As a matter of fact, by means of a simple numerical analysis, we have been able to determine which is the suitable number of measurement to perform as well as the number of working frequencies to consider.

REFERENCES

[1] **Daniels, D. J.,** 1996. Subsurface Penetrating Radar, IEEE Press, New Jersey.

[2] **Deming, R. W., and Devaney, A. J.,** 1997. Diffraction tomography for multi-monostatic ground penetrating radar imaging, *Inverse Problems, 13, 29-45.*

[3] **Lesselier, D. and Duchene, B.,** 1996. Wavefield inversion of objects in stratified environments. From backpropagation schemes to full solutions, in *Radio Science 1993-1996,235-268,* Ed. Stone, R., Oxford University Press, Oxford.

[4] **Colton, D. And Kress, R.** 1992. Inverse acoustic and electromagnetic scattering, Springer Verlag, Berlin.

[5] **Bucci, O. M. and Isernia, T.,** 1997. Electromagnetic inverse scattering: retrievable information and measurement strategies, *Radio Science, 32,2123-2138.*

[6] **Pierri, R. and Leone, G.,** 1999. Inverse scattering of dielectric cylinders by a second order Born approximation, *IEEE Trans. Geosci. Rem. Sens., 37, 374-382*.

[7] **Bertero, M. and Boccacci, P.,** 1998. Introduction to Inverse Problems In Imaging, Inst. Of Physics, Bristol & Philadelphia, UK.

[8] **Isernia, T., Pascazio, V. and Pierri, R.,** 1997. A non-linear estimation method in tomographic imaging, *IEEE Trans. Geosci. Rem. Sens., 35, 910-923*.

[9] **Kleinman, R. E. and van den Berg, P. M.,** 1993. An extended-range modified gradient technique for profile inversion, *Radio Science, 28, 877-884*.

[10] **Leone, G., Brancaccio, A. and Pierri, R.,** 2001. The quadratic distorted approximation for the inverse scattering of dielectric cylinders, *J. Opt. Soc. Am., Pt. A, 18, 600-609.*

[11] **Isernia, T., Pascazio, V. and Pierri, R.,** 2001. On the local minima in a tomographic imaging technique, *IEEE Trans. Geosci. Rem. Sens., 39, 1596-1607*.

[12] **Pierri, R,. Leone, G., Persico, R. and Soldovieri, F., 2001**. Electromagnetic inversion for subsurface applications under the distorted Born approximation, *Il Nuovo Cimento Sez. C, 24C, n. 2, 245-261*

[13] **Pierri, R., Brancaccio, A., Leone, G. and Soldovieri, F.,** 2002. Electromagnetic prospection via homogeneous and inhomogeneous plane waves: the case of an embedded slab, *AEÜ, International Journal of Electronics and Communications, 56, n. 1, 11-18*.

[14] **Wang, T., and Oristaglio, M.,** 2000. GPR imaging using the generalized Radon transform, *Geophysics, 65, pp 1553-1559.*

[15] **Slaney, M., Kak, A. C. and Larsen, L. E.,** 1984. Limitations of imaging with first-order diffraction tomography, *IEEE Trans. Microwave Theory Tech., MTT-32, 860-874.*

[16] **Bucci, O. M., Crocco, L., Isernia, T. and Pascazio, V.,** 2001. Subsurface inverse scattering problems: quantifying qualifying and achieving the available information, *IEEE Trans. Geosci. Rem. Sens., 39, 2527-2538*.

[17] **Pierri, R., Liseno, A., Solimene, R. and Soldovieri, F.,** 2002. Resolution limits in the Fresnel zone: roles of aperture and frequency, *Subsurface Sensing Technologies and Applications, 3, n. 1, pp. 1-18*.

[18] **Crocco, L., Persico, R. and Soldovieri, F.**, 2002. A tomographic approach for imaging targets embedded in a layered medium, *Proc. 9th International Conference on Ground Penetrating Radar, GPR 2002,* Santa Barbara, CA, USA.

[19] **Chew, W. C.,** 1995. Waves and Fields in Inhomogeneous Media, IEEE Press, New Jersey.

[20] **Bucci, O. M., Cardace, N., Crocco, L. and Isernia, T.,** 2001. Degree of non-linearity and a new solution procedure in scalar 2-d inverse scattering problems, *J. Opt. Soc. Am. A, 18, 1832-1845.*

[21] **Richmond, J. H.,** 1965. Scattering by a dielectric cylinder of arbitrary cross section shape, *IEEE Trans. Antennas and Propagat., 13, pp. 334-341*.

[22] **Crocco, L. and Soldovieri, F.,** 2003. GPR prospecting in a layered medium via microwave tomography, *Annals of Geophysics, **46, 3,** pp 559-572.*

BIOGRAPHY

Evrim Tetik was born in Çanakkale, Turkey in 1978. She received the B.Sc. degree in electronics and communication engineering from Istanbul Technical University. In 2005, she became a research assistant at the same department. She is currently working toward the M.Sc. degree at Istanbul Technical University.